Intracellular Acoustic Droplet Vaporization in a Single Peritoneal Macrophage for Drug Delivery Applications

ARTICLE *in* LANGMUIR · SEPTEMBER 2011

Impact Factor: 4.46 · DOI: 10.1021/la203212p · Source: PubMed

2 AUTHORS, INCLUDING:

Shih-Tsung Kang
National Tsing Hua University
27 PUBLICATIONS **182** CITATIONS

Langmuir

ARTICLE

pubs.acs.org/Langmuir

Intracellular Acoustic Droplet Vaporization in a Single Peritoneal Macrophage for Drug Delivery Applications

Shih-Tsung Kang and Chih-Kuang Yeh*

Department of Biomedical Engineering and Environmental Sciences, National Tsing Hua University, 101, Section 2, Kuang-Fu Road, Hsinchu, Taiwan 30013

Supporting Information

ABSTRACT: This study investigated the acoustic droplet vaporization (ADV) of perfluoropentane (PFP) droplets in single droplet-loaded macrophages (DLMs) by insonation with single three-cycle ultrasound pulses. Transient responses of intracellular ADV within a single DLM were observed with synchronous high-speed photography and cavitation detection. Ultrasound B-mode imaging was further applied to demonstrate the contrast enhancement of ADV-generated bubbles from a group of DLMs. The PFP droplets incorporated in a DLM can be liberated from the cell body after being vaporized into gas bubbles. Inertial cavitation can be simultaneously induced at the same time that bubbles appear. The coalescence of bubbles occurring at the onset of vaporization may facilitate gas embolotherapy and ultrasound imaging. Macrophages can be potential carriers transporting PFP droplets to avascular and hypoxic regions in tumors for ultrasound-controlled drug release and ADV-based tumor therapies.

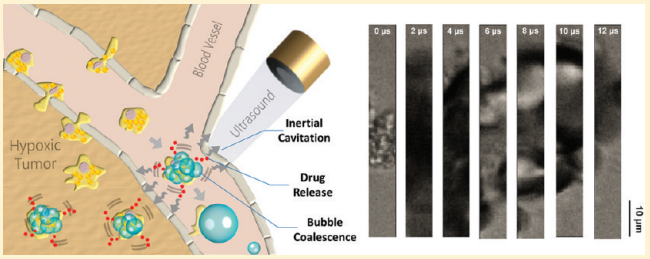

INTRODUCTION

Recent studies have demonstrated that ultrasound sonication can vaporize superheated perfluorocarbon (PFC) droplets into gaseous bubbles via acoustic droplet vaporization (ADV).[1] This technique can generate bubbles to promote vascular occlusion[2] and ultrasound ablation[3] for tumor treatments, and liberate the encapsulated chemotherapeutic agents for ultrasound-mediated drug delivery.[4,5] ADV may occur with inertial cavitation (IC) when the applied acoustic pressure is higher than a particular threshold. This threshold pressure varies with acoustic properties such as pulse duration and pulse repetition frequency, droplet parameters such as size and degree of superheat, and bulk fluid properties such as gas saturation, viscosity, and surface tension.[6] Many studies have shown that both IC and stable cavitation improve the efficacy of drug delivery by facilitating the dispersion of drug molecules and increasing the permeability of blood vessels and cell membranes.[7,8] With these features, ADV shows great promise in tumor therapy. However, solid tumors normally possess hypoxic areas and abnormal vasculature with higher interstitial fluid pressure than adjacent normal tissue. These properties reduce the transfer of drugs (in particular, macromolecules and large particles) into the tumors, resulting in the resistance of tumors to chemotherapy.[9] Recent studies have shown that monocytes and derived macrophages can be engineered to actively migrate toward tumors and infiltrate avascular and hypoxic areas.[10] This prompted us to propose the use of droplet-loaded macrophages (DLMs) in ADV-based tumor therapies.

Several studies have demonstrated the properties of phagocytosed bubbles in macrophage-like cells. These bubbles remain acoustically active and are capable of exhibiting large volumetric oscillation in response to an acoustic pulse.[11] Cells membranes can be permeabilized or damaged above a threshold pressure lower than that needed to induce free-field inertial cavitation.[12,13] However, no study investigates the optical and acoustic dynamics of phagocytosed PFC droplets during ADV. There are two major differences between the ADV happening within single DLMs and in a freely distributed suspension. The viscosity of cytoplasm (2−3 mPa·s) is greater than that of water (0.7 mPa·s). Bulk fluids of higher viscosity reportedly result in higher ADV and IC pressure thresholds.[6] In addition, local number density of droplets within a DLM may be far above that in a suspension. Whether and how ADV occurs in living cells needs to be investigated. Considering that the DLMs in a tumor might have a low density and that reduced energy deposition in biological tissue may be preferable for this technique in clinical use, we investigated the feasibility of using single three-cycle ultrasound pulses to induce ADV within single DLMs. Transient responses of intracellular ADV were observed with synchronous high-speed photography and cavitation detection. Ultrasound imaging was further applied to demonstrate the contrast enhancement of ADV-generated bubbles from a group of DLMs. The physical responses of DLMs to ultrasound sonication such as bubble generation, cell membrane disruption, and IC activity were observed to assess the possible usefulness of this technique in clinical applications.

Received: August 17, 2011
Revised: September 15, 2011
Published: September 21, 2011

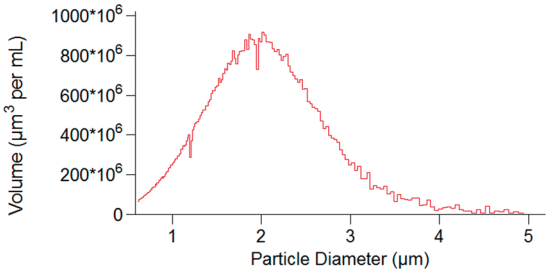

Figure 1. Volumetric size distribution of homemade PFP droplets.

EXPERIMENTAL SECTION

PFC Droplet Preparation. PFC droplets were composed of perfluoropentane (PFP, 29 °C bulk boiling point), phospholipids, and fluorescent dye DiI. The materials were purchased from ABCR GmbH & Co. KG (Karlsruhe, Germany), Avanti Polar Lipids Inc. (AL, USA), and Sigma−Aldrich Co. (MO, USA), repectively. A thin lipid film containing 94.8 mol % distearoylphosphatidylcholine (DSPC), 5 mol % distearoylphosphatidylethanolamine-poly(ethylene glycol)2000 (DSPE-PEG2000), and 0.2 mol % DiI was prepared in a 2 mL vial according to the procedures described in our previous study.[14] One milliliter of degassed and sterile phosphate-buffered saline (PBS, 20 mM, pH 7.4) was added to the vial to dissolve the lipid film. One hundred microliters of PFP was then injected into the vial using a 100 μL gastight syringe (HA-81000, Hamilton Co., Tokyo, Japan). Note that both the syringe and vial with PBS was kept in an ice bath before use to avoid the evaporation of PFP. Droplet emulsions were formed by immersing the vial in a sonication bath at 20 °C for 15 min. Nonencapsulated DiI was removed by four washing/centrifugation cycles with clean PBS. The droplet yield was measured with a Coulter counter (model Multisizer 3, Beckman Coulter Inc., CA, USA) to be $(3-5) \times 10^{10}$ droplets/mL within the size range of 0.6 to 5.0 μm. The mean diameter in volumetric size distribution was 2.26 ± 0.19 μm (mean ± SD, $N = 6$), as shown in Figure 1.

DLM Preparation. Normal macrophages (NMs) were isolated from the peritoneal cavity of C57BL mice according to the reported procedures.[15,16] The mice were purchased from the National Laboratory Animal Center (Taipei, Taiwan), and bred in National Tsing Hua University Laboratory Animal Center (Hsinchu, Taiwan). The handling of the mice was conducted with the approval of Institutional Animal Care and Use Committee (IACUC approval number: 09508). The recruitment of NMs in each mouse was stimulated by an intraperitoneal injection of 3 mL of 3% thioglycolate (Sigma−Aldrich Co., MO, USA). Four days later, the peritoneal cavity of each mouse was lavaged by 3 mL of sterile PBS twice following sacrifice via CO_2 inhalation. The lavage fluid that normally contained up to 1×10^7 thioglycolate-elicited NMs for each mouse was collected and then centrifuged at 400 g (1500 rpm) for 5 min to discard the supernatant. The cell pellet was resuspended in RPMI 1640 medium, and cultured overnight to remove nonadherent (i.e., nonmacrophage) cells. For attaining DLMs, 2.5×10^5 NMs were plated in each well of a 6-well tissue culture plate for adherence for 1 day, and were then incubated with 1×10^7 PFP droplets at 37 °C in a 5% CO_2 incubator. Adherent NMs gradually incorporated PFP droplets to become adherent DLMs. After 4 h of incubation, the wells were rinsed by PBS to remove nonincorporated droplets. DLMs were harvested and centrifuged to discard the supernatant that contained cell debris. Collected DLMs were resuspended in RPMI 1640 medium, and then kept in an ice bath before being used in subsequent experiments.

DLM Assessment. Bright field and fluorescence microscopy of these cells was performed with an inverted microscope (model IX71, Olympus Corp., Tokyo, Japan) equipped with a CCD camera (model DP72, Olympus Corp., Tokyo, Japan). Cell uptake efficiency and cell viability were measured by flow cytometry assay (BD FACSCanto, BD Biosciences, NJ, USA) with propidium iodide (PI) staining. To validate the ability of DLMs to deliver the internalized PFP droplets, transmembrane cell migration assays were performed to examine the migration mobility of DLMs in comparison with that of NMs.[17] A cup-shaped insert (no. 353097, BD Falcon, NJ, USA) with a porous polycarbonate membrane on its bottom was placed in the well of a 24-well tissue culture plate. Each well of the tissue culture plate was filled with the conditioned medium of transgenic adenocarcinoma of the mouse prostate cells prepared according to the reported procedures.[18] The conditioned medium served as a chemoattractant to recruit macrophages. Approximately 50 000 DLMs or NMs (as assessed by hemocytometer and Trypan blue stain) were seeded on the top of the membrane. The average pore size in the membrane was approximately 8 μm, which enabled cell migration through the membrane. The amounts of DLMs and NMs which migrated through the membrane were quantified after 6 h of incubation at 37 °C. This incubation time was chosen since it has been suggested in several studies for obtaining sufficient migration efficiency.[19,20]

High-Speed Photography and Cavitation Detection. The ADV experiments were conducted in an integrated acousto-optical system, based on the system proposed by Dayton et al.[21], as illustrated in Figure 2. A high-speed camera (model FASTCAM SA4, Photron Ltd., Tokyo, Japan) capable of operating at capture rates up to 500 000 fps was interfaced to an inverted microscope (model IX71, Olympus Corp., Tokyo, Japan) attached to a custom-designed water tank. The tank was filled with degassed and deionized water that was maintained at 37 °C to simulate body temperature. A 2 MHz high-intensity focused ultrasound (HIFU) transducer (model SU-101, Sonic Concepts Inc., WA, USA) with a −6 dB bandwidth of 52% was placed in the tank and confocally positioned with a water-immersion objective (model Achroplan 40×, Carl Zeiss Ltd., Tokyo, Japan). The transducer was driven by a three-cycle signal generated by an arbitrary waveform generator (model AWG 2005, Tektronix Inc., CA, USA) and amplified by a 53 dB radiofrequency (RF) power amplifier (model A150, E&I Ltd., NY, USA) to transmit vaporization pulses at a peak negative pressure of 8 MPa. The acoustic pressure was calibrated with an 85-μm-diameter hydrophone (model HGL-0085, Onda Corp., CA, USA) in degassed and deionized water. Furthermore, a 200-μm-diameter vessel-mimicking cellulose tube (Spectrum Laboratories. Inc., CA, USA) was positioned at the optical focus. DLMs were injected into the tube and regulated to the optical focus with a manual microinjector (model IM-6, Narishige Co., Tokyo, Japan) to be exposed to single vaporization pulses. A homemade $LiNbO_3$ 40 MHz transducer with a −6 dB bandwidth of 60% MHz was used for passive cavitation detection (PCD) and active cavitation detection (ACD) for monitoring the generation of bubbles and IC, respectively. For PCD, the transducer was operated in the receive mode, whereas for ACD, it was operated in a pulse echo mode. In pulse echo mode, a 120 cycle and 700 kPa interrogation pulse was timed to reach the mutual focus simultaneously with the vaporization pulse. The signal driving the transducer was generated by an arbitrary waveform generator (model AWG 2041, Tektronix Inc., CA, USA), and amplified by a 50 dB RF power amplifier (model 325LA, E&I Ltd., NY, USA). The switch between ACD and PCD modes was conducted by turning the waveform output on and off, respectively, on the arbitrary waveform generator. Note that both beam axes of the two transducers were perpendicular to the cellulose tube to minimize the attenuation of transmitted and backscattered ultrasound energy. In each experimental run, only one DLM was insonated within the beam area of the 40 MHz transducer. One RF signal was synchronously acquired through a diode limiter/transformer diplexer circuit (model DIP-3, Matec Instruments NDT Inc., MA, USA), which protects receive circuitry from high voltages required for transmission. The acquired signal was amplified by a pulser/receiver (model 5073PR, Olympus NDT Inc., MA, USA), and then digitized by an oscilloscope (model LT354, LeCroy Corp., NY, USA) at a sampling rate of 1 Gsample/s. The digitized signal

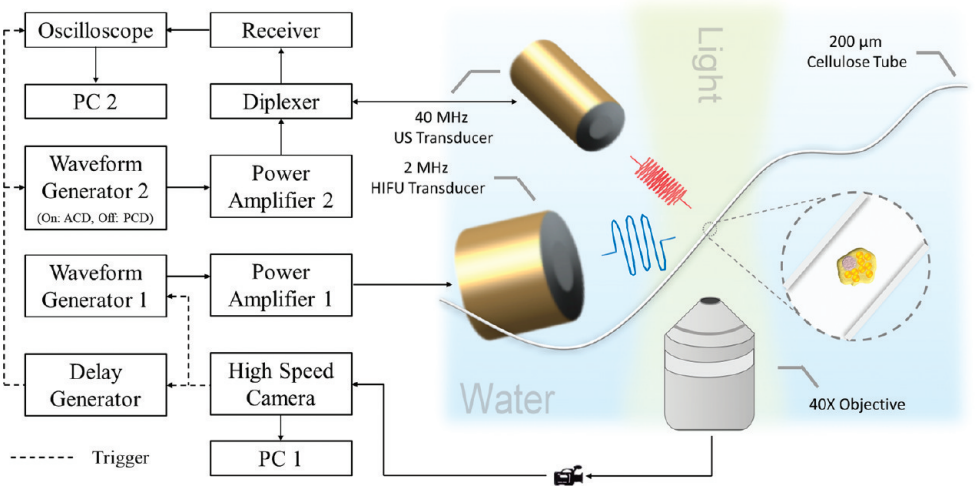

Figure 2. Schematic diagram of an integrated acousto-optical system for synchronous high-speed photography and cavitation detection.

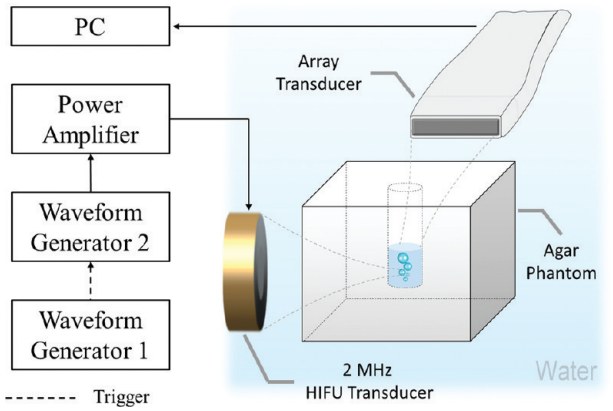

Figure 3. Experimental setup of ultrasound B-mode imaging.

was sent to a computer via GPIB, and then processed off-line using *MATLAB* (MathWorks Inc., MA, USA) software. In the system, all the triggers were synchronized with that initiated from the high-speed camera. A digital delay generator (model DG535, Stanford Research Systems Inc., CA, USA) was used to regulate the trigger delay between the two waveform generators for the simultaneous arrival of vaporization and interrogation pulses at the mutual focus.

Ultrasound Imaging of ADV-Generated Bubbles. Ultrasound B-mode imaging was further applied to demonstrate the contrast enhancement of ADV-generated bubbles from a population of DLMs. Two kinds of samples were prepared in 300 μL PBS: one was 1.9×10^7 free PFP droplets (FDs) preincubated with 1.3×10^5 NMs; the other was 1.9×10^7 FDs alone, which served as a control. Nonincorporated PFP droplets were not rinsed off in order to achieve equal amounts of droplets in these two samples. The experimental setup is illustrated in Figure 3. The samples were poured into a cylindrical chamber in an acoustically transparent phantom constructed by solidified agarose gel (Invitrogen Co., CA, USA) at a concentration of 2 wt %. The same vaporization pulses were used to continuously induce intracellular ADV at a pulse repetition frequency of 10 Hz. ADV-generated bubbles were imaged above the sonication site using a clinical ultrasound imaging system equipped with a 128 element linear array probe (model t3000, Terason, MA, USA). Note that the beam axis of the probe was aligned perpendicular to that of the HIFU transducer to minimize possible signal interference in acquired images. The data were processed and analyzed using *MATLAB*.

RESULTS AND DISCUSSION

DLM Assessment. Bright-field and fluorescence microscopy images of PFP droplets and of harvested single DLM and NM are presented in Figure 4a, where the increasing granularity and fluorescence in the cell body indicate the uptake of PFP droplets. Time-course microscopy showed no evident vaporization of the intracellular PFP droplets during at least 24 h of incubation at 37 °C. Flow cytometric analysis showed that the averaged cell uptake efficiency was 83.1 ± 6.8% (mean ± SD, N = 5), indicating that most adherent NMs on the tissue culture plate were loaded with PFP droplets after 4 h incubation. The amount of PI positive cells was less than 1% of the whole population, indicating that no cell apoptosis resulted from the uptake of PFP droplets. In the transmembrane migration assays, the cells slowly migrated toward the opposite side of the membrane through the 8 μm pores during 6 h of incubation (Figure 4b). The amounts of migratory DLMs and NMs were 237 ± 46 cells/mm^2 and 254 ± 40 cells/mm^2 (N = 5), respectively, with a p-value of 0.3. This indicates that the migration mobility of DLMs was comparable to that of the NMs. Although the DLMs had sizes of up to 20 μm, they might not cause acute vascular occlusion, particularly at the hepatic and pulmonary capillaries *in vivo*. It has been reported that the accumulation of human macrophages (with a mean size of 21.2 μm)[22] was high in the hypoxic tumor but low in the lung of the athymic mice in 48 h, probably owing to the deformability of macrophages.[10] Note that the deformability of DLMs has also been validated by the transmembrane cell migration assays.

High-Speed Photography. The image frames in Figure 5a show the occurrence of ADV in a single DLM exposed to a single vaporization pulse. The high-speed camera was initially operated at a lower capture rate (100 000 fps) to obtain larger image size (192 × 128 pixels) for the overview of intracellular ADV. The PFP droplets packed inside the DLM underwent a phase transition into gas bubbles that subsequently disrupted the cell membrane and exploded out of the cell body. Some of the bubbles remained in the cell debris, indicating that organelles retarded their mobility (Supporting Information, Video S1). Some nonvaporized PFP droplets were also found in the cell debris, which may be attributed to the packed droplets shielding each other from ultrasound exposure. A similar phenomenon was found in the disruption of packed bubbles by ultrasound.[14]

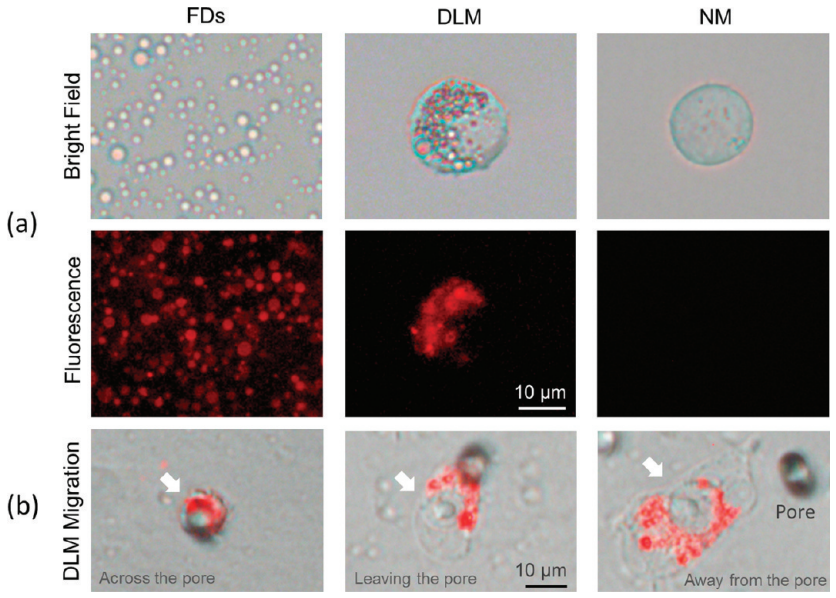

Figure 4. (a) Bright-field and fluorescence microscopy images of FDs and of a harvested single DLM and NM. The six images are on the same scale. (b) Merged bright-field and fluorescence microscopy images of migratory DLMs in three different stages. The arrow denotes the location of DLM. The three images are on the same scale.

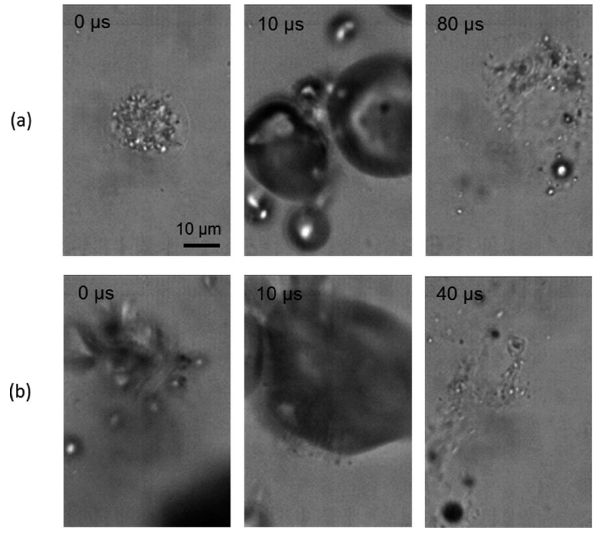

Figure 5. High-speed images of a single DLM exposed to the first (a) and second (b) vaporization pulses.

However, applying a subsequent pulse facilitated the liberation of the stuck bubbles, and these bubbles could presumably act as cavitation nuclei facilitating the ADV of the residual PFP droplets (Figure 5b). Afterward, fewer granular particles were found in the cell debris. These results indicate that most internalized PFP droplets can be released from DLMs by insonation with a few vaporization pulses.

Synchronous High-Speed Photography and Cavitation Detections. The high-speed camera was then operated at a higher capture rate (500 000 fps) and synchronized with cavitation detection to assess the physical responses of a single DLM to a single vaporization pulse. The image frames in Figure 6a suggest that the onset of intracellular ADV was a transient process with a duration of less than 2 μs. The blurred images at 2 and 4 μs indicate the acute motion of ADV-generated bubbles. These bubbles were much larger (30−40 μm, also seen in Figure 5a) than those predicted by the reported 5-fold expansion if the incorporated PFP droplets had diameters of 1−2 μm.[1] This indicates that significant bubble coalescence occurred after the onset of intracellular ADV. Many studies have suggested that this phenomenon (for free-field ADV) is driven by the tendency to reduce the increased surface tension in response to the decreased surface density of surfactant molecules,[23] and can be promoted by secondary Bjerknes radiation forces between bubbles.[24] Within a DLM, this phenomenon may be further facilitated by the high number density of the incorporated PFP droplets due to the space constraint of the cell membrane. The synchronously acquired ACD signals for the DLM and a NM are shown in Figure 6b. Three distinct peaks in the baseline signal arose from the harmonic leakage of the echo of the vaporization pulse due to the oscillation of the cellulose tube. However, the increase in amplitude after 1.5 μs indicates the presence of ADV-generated bubbles after the second cycle of insonation of the vaporization pulse. The time-vs-frequency plot of the PCD signal acquired for another DLM and NM showed a broadband noise generated at the same time that bubbles appeared (Figure 6c). This resulted in a 17.69 $\pm$ 7.35% increase in the integrated amplitude of the averaged Fourier spectrum for single DLMs than that for single NMs (N = 10). These results indicate the presence of IC simultaneously with the appearance of ADV-generated bubbles during intracellular ADV for a DLM exposed to an 8 MPa vaporization pulse. The IC event may arise from the acute volume growth and coalescence of vaporized droplets, and simultaneous interaction between the resultant bubbles and vaporization pulse. In most cases, the IC activity was usually less evident in the third cycle than in the second cycle. We speculate that bubbles in the third cycle stopped expanding and had thoroughly coalesced into large bubbles, which predictably required much higher acoustic pressure to exhibit IC.[6] Note that IC might not happen with intracellular ADV if driven at lower acoustic pressure, since it has been demonstrated that the threshold pressure to induce free-field ADV is normally lower than that to induce both free-field ADV and

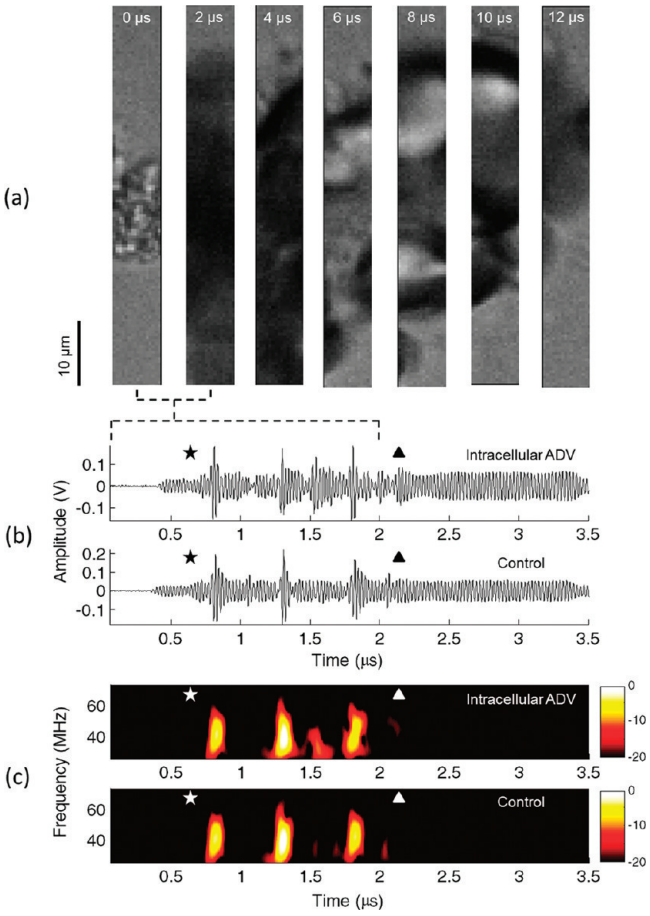

Figure 6. (a) High-speed images of a single DLM exposed to a single vaporization pulse. (b) Corresponding ACD signals with (top) and without (bottom) intracellular ADV. (c) Examples of PCD signals with (top) and without (bottom) intracellular ADV. The star and triangle indicate the beginning and end of the vaporization pulse, respectively.

IC.[6] Also note that intracellular ADV might not necessarily happen in the second cycle when different transducers and acoustic pulses were used. The acoustic pressures of the first and third cycles of the transmitted pulse were relatively lower (~6 MPa) in comparison with that of the second cycle due to limited bandwidth.

Ultrasound Imaging of ADV-Generated Bubbles. The results showed that the continuously generated ADV bubbles floated up and increased the signal-to-noise ratio (SNR) in the acquired B-mode images as a function of time (Figure 7a). At every time point, the bubbles resulting from the FDs preincubated with NMs produced much higher acoustic intensity than that from FDs alone, even at half the original concentration (Figure 7b). These results support the role of DLMs to facilitate the generation of large bubbles, which may benefit vascular occlusion for gas embolotherapy that conventionally utilizes FDs.[2] Furthermore, since the intensity of ultrasound echoes from a point scatterer is proportional to the sixth power of the particle diameter based on Rayleigh scattering, larger bubbles could produce much higher contrast enhancement in ultrasound images than the smaller ones. Therefore, bubble coalescence may increase the possibility to detect the intracellular ADV events of single DLMs or a small numbers of DLMs *in vivo*. This is particularly advantageous for clinical applications when the number of migratory DLMs within a tumor is low.

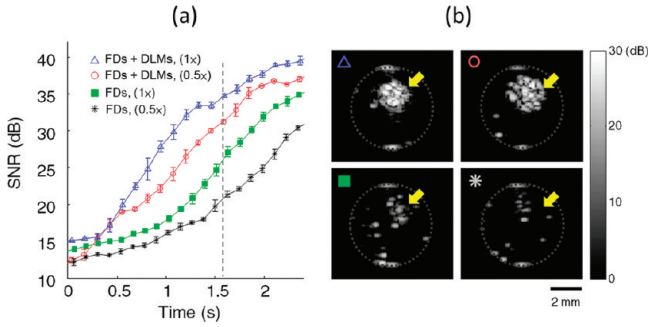

Figure 7. (a) SNR increased by ADV-generated bubbles as a function of time for 4 different samples in 300 μL of PBS buffer: 1.9×10^7 FDs alone (square, FDs, 1×), 1.9×10^7 FDs preincubated with 1.3×10^5 NMs for 4 h (triangle, FDs+DLMs, 1×), and the same cases at half the original concentration (asterisk, FDs, 0.5×; circle, FDs+DLMs, 0.5×). (b) B-mode images of the 4 cases at 1.6 s. The arrow denotes the point above the sonication site.

The concentration of droplets within a DLM is far above that in a freely distributed suspension. For comparison, the concentration of droplet suspension used by Fabiilli et al. was 9×10^4 droplets/mL.[6] Assuming that the size of a macrophage is 1000 μm^3, the equivalent number of droplets within a DLM will be far less than one droplet.[22] However, each DLM was able to deliver tens of droplets to hundreds of droplets. The shielding of ultrasound energy might be significant among the incorporated droplets. In addition, the high viscosity of cytoplasm might result in the increase in ADV threshold pressure.[6] Since investigating the specific threshold pressure for inducing the intracellular ADV is beyond the focus of this study, a fairly high acoustic pressure (8 MPa) was used throughout the experiments. Although the mechanical index was much higher than 1.9 (FDA regulatory limit for diagnostic ultrasound equipment), it was in the range of those used in some clinical and preclinical ultrasound therapeutic applications (e.g., drug delivery, lithotripsy, histotripsy, and HIFU ablation).[25] Nevertheless, there are several methods for reducing the ADV threshold pressure, such as increasing droplet size, pulse duration, and ultrasound frequency.[1,6] Recently, a new technique has been reported to fabricate droplets with lower boiling PFCs (such as perfluorobutane, C_4F_{10}) than PFP.[26] These droplets can be vaporized by insonation with short ultrasound pulses at a MI of 1.2. This approach may potentially lower the MI of applied acoustic pulses for intracellular ADV to the diagnostic ultrasound range.

CONCLUSIONS

In conclusion, we have demonstrated the feasibility of inducing ADV in single DLMs by insonation with single three-cycle ultrasound pulses to liberate the incorporated PFP droplets. The PFP droplets vaporized within single DLMs can coalesce to form large bubbles upon the onset of vaporization. When an 8 MPa vaporization pulse is used, an IC event can be simultaneously induced upon the occurrence of bubbles, presumably in the early stage of bubble coalescence. Since the IC of bubbles has been reported to aid drug extravasation and bubble coalescence may benefit vascular occlusion, the use of DLMs to transport PFP droplets toward tumors shows great promise for advancing the development of both drug delivery and ADV-based tumor therapies. The use of ultrasound triggering permits controlled drug release. Future studies should investigate the effects of the

amount and sizes of incorporated droplets on the amount of ADV-liberated drug payload, and on the infiltration ability of the DLMs *in vivo*.

■ ASSOCIATED CONTENT

Supporting Information. The video version of Figure 5. This material is available free of charge via the Internet at http://pubs.acs.org.

■ AUTHOR INFORMATION

Corresponding Author
*Phone: +886-3-5715131 ext 34240, Fax: +886-3-5718649, E-mail: ckyeh@mx.nthu.edu.tw.

■ ACKNOWLEDGMENT

The authors acknowledge the National Science Council of Taiwan for the grants (NSC 99-2628-E-007-001 and 100-2627-M-007-004), Professors C.-S. Chiang and Y.-F. Huang for their preparation of normal macrophages, and C.-H. Wang for his contribution to droplet fabrication.

■ REFERENCES

(1) Kripfgans, O. D.; Fowlkes, J. B.; Miller, D. L.; Eldevik, O. P.; Carson, P. L. *Ultrasound Med. Biol.* **2000**, *26*, 1177–1189.
(2) Zhang, M.; Fabiilli, M. L.; Haworth, K. J.; Fowlkes, J. B.; Kripfgans, O. D.; Roberts, W. W.; Ives, K. A.; Carson, P. L. *Ultrasound Med. Biol.* **2010**, *36*, 1691–1703.
(3) Zhang, P.; Porter, T. *Ultrasound Med. Biol.* **2010**, *36*, 1856–1866.
(4) Rapoport, N. Y.; Kennedy, A. M.; Shea, J. E.; Scaife, C. L.; Nam, K. H. *J. Controlled Release* **2009**, *138*, 268–276.
(5) Fabiilli, M. L.; Haworth, K. J.; Sebastian, I. E.; Kripfgans, O. D.; Carson, P. L.; Fowlkes, J. B. *Ultrasound Med. Biol.* **2010**, *36*, 1364–1375.
(6) Fabiilli, M. L.; Haworth, K. J.; Fakhri, N. H.; Kripfgans, O. D.; Carson, P. L.; Fowlkes, J. B. *IEEE Trans. Ultrason. Ferroelectr. Freq. Control* **2009**, *56*, 1006–1017.
(7) Pitt, W. G.; Husseini, G. A.; Staples, B. J. *Expert Opin. Drug Delivery* **2004**, *1*, 37–56.
(8) Sundaram, J.; Mellein, B. R.; Mitragotri, S. *Biophys. J.* **2003**, *84*, 3087–3101.
(9) Chen, S. T.; Pan, T. L.; Juan, H. F.; Chen, T. Y.; Lin, Y. S.; Huang, C. M. *J. Proteome Res.* **2008**, *7*, 1379–1387.
(10) Muthana, M.; Giannoudis, A.; Scott, S. D.; Fang, H. Y.; Coffelt, S. B.; Morrow, F. J.; Murdoch, C.; Burton, J. L.; Cross, N.; Burke, B.; Mistry, R.; Hamdy, F.; Brown, N. J.; Georgopoulos, L.; Hoskin, P. J.; Essand, M.; Lewis, C. E.; Maitland, N. J. *Cancer Res.* **2011**, *71*, 1805–1815.
(11) Dayton, P. A.; Chomas, J. E.; Lum, A. F. H.; Allen, J. S.; Lindner, J. R.; Simon, S. I.; Ferrara, K. W. *Biophys. J.* **2001**, *80*, 1547–1556.
(12) Miller, D. L.; Quddus, J. *IEEE Trans. Ultrason. Ferroelectr. Freq. Control* **2002**, *49*, 1094–1102.
(13) Miller, D. L.; Dou, C. *Ultrasound Med. Biol.* **2004**, *30*, 973–977.
(14) Kang, S. T.; Yeh, C. K. *Ultrason. Sonochem.* **2011**, *18*, 327–333.
(15) Chiang, C. S.; Chen, F. H.; Hong, J. H.; Jiang, P. S.; Huang, H. L.; Wang, C. C.; McBride, W. H. *Int. Immunol.* **2008**, *20*, 215–222.
(16) Shirey, K. A.; Cole, L. E.; Keegan, A. D.; Vogel, S. N. *J. Immunol.* **2008**, *181*, 4159–4167.
(17) Hulkower, K. I.; Herber, R. L. *Pharmaceutics* **2011**, *3*, 107–124.
(18) Zhao, D.; Najbauer, J.; Garcia, E.; Metz, M. Z.; Gutova, M.; Glackin, C. A.; Kim, S. U.; Aboody, K. S. *Mol. Cancer Res.* **2008**, *6*, 1819–1829.
(19) Barlow, P. G.; Clouter-Baker, A.; Donaldson, K.; Maccallum, J.; Stone, V. *Part. Fibre Toxicol.* **2005**, *2*, 11.
(20) Gong, Y.; Hart, E.; Shchurin, A.; Hoover-Plow, J. *J. Clin. Invest.* **2008**, *118*, 3012–3024.
(21) Dayton, P. A.; Morgan, K. E.; Klibanov, A. L.; Brandenburger, G. H.; Ferrara, K. W. *IEEE Trans. Ultrason. Ferroelectr. Freq. Control* **1999**, *46*, 220–232.
(22) Krombach, F.; Münzing, S.; Allmeling, A. M.; Gerlach, J. T.; Behr, J.; Dörger, M. *Environ. Health Perspect.* **1997**, *105*, 1261–1263.
(23) Rapoport, N. Y.; Efros, A. L.; Christensen, D. A.; Kennedy, A. M.; Nam, K.-H. *Bubble Sci. Eng. Technol.* **2009**, *1*, 31–39.
(24) Haworth, K. J.; Kripfgans, O. D. *IEEE Int. Ultrason. Symp. Proc* **2008**, 623–626.
(25) Shaw, A.; Hodnett, M. *Ultrasonics* **2008**, *48*, 234–252.
(26) Sheeran, P. S.; Luois, S.; Dayton, P. A.; Matsunaga, T. O. *Langmuir* **2011**, *27*, 10412–10420.